




# Outer Wall Segmentation of Abdominal Aortic Aneurysm by Variable Neighborhood Search Through Intensity and Gradient Spaces

Thanongchai Siriapisith<sup>1,2</sup> · Worapan Kusakunniran<sup>2</sup>  · Peter Haddawy<sup>2</sup>

Published online: 19 January 2018

© Society for Imaging Informatics in Medicine 2018

## Abstract

Aortic aneurysm segmentation remains a challenge. Manual segmentation is a time-consuming process which is not practical for routine use. To address this limitation, several automated segmentation techniques for aortic aneurysm have been developed, such as edge detection-based methods, partial differential equation methods, and graph partitioning methods. However, automatic segmentation of aortic aneurysm is difficult due to high pixel similarity to adjacent tissue and a lack of color information in the medical image, preventing previous work from being applicable to difficult cases. This paper uses a variable neighborhood search that alternates between intensity-based and gradient-based segmentation techniques. By alternating between intensity and gradient spaces, the search can escape from local optima of each space. The experimental results demonstrate that the proposed method outperforms the other existing segmentation methods in the literature, based on measurements of dice similarity coefficient and jaccard similarity coefficient at the pixel level. In addition, it is shown to perform well for cases that are difficult to segment.

**Keywords** Abdominal aortic aneurysm · Computed tomography · Multi-layer segmentation · Iterative · Graph cut · Variable neighborhood search · Probabilistic model

## Introduction

The aorta is the largest vessel in the human body. It is tubular in shape, emanating from the heart in the chest and passing into the abdomen to supply blood to all organs in the body. Aortic aneurysm is a dilatation of the aorta, which can cause rupture leading to death. Epidemiological studies in the USA have revealed that abdominal aortic aneurysm (AAA) is a disease of increasing incidence and mortality, with major risk factors being hypertension, high cholesterol and smoking [1, 2]. More than 10,000 people die from rupture each year [3, 4]. While aortic aneurysm can occur

in the thorax or abdominal area, rupture is more common in the abdominal region [3].

The aorta is composed of inner and outer walls. The normal diameter of the aorta is typically not larger than 30 mm, with a patient considered to have an aneurysm when the absolute diameter is increased more than 1.5 times of the normal diameter. In general, the maximum cross section diameter (outer to outer wall) is related to risk of rupture due to increased wall tension with increased radial growth. The risk of rupture is defined to be high when the maximum diameter is greater than 5.5 cm and the rate of increase is more than 1 cm/year [5]. The peak wall stress has shown more reliability to predict rupture and is highly dependent on the aneurysm shape [6]. A 3D model of aneurysm can be used to calculate peak wall stress. In the literature, such models have been built using the segmented aneurysm in medical images via manual, automatic, or semi-automatic processes. However, manual delineation is a time consuming process that requires more than an hour for each case.

In addition, because of slow and turbulent flow, blood clots or thrombus are commonly found in aneurysms separating outer wall from inner wall. During aneurysm growth, the outer wall expands and the thrombus formation

---

✉ Worapan Kusakunniran  
worapan.k@hotmail.com

Thanongchai Siriapisith  
thanongchai@gmail.com

Peter Haddawy  
haddawy@gmail.com

<sup>1</sup> Department Radiology, Faculty of Medicine Siriraj Hospital, Mahidol University, Bangkok, 10700, Thailand

<sup>2</sup> Faculty of Information and Communication Technology, Mahidol University, Nakhon Pathom, 73170, Thailand

progressively increases non-uniformly. For this reason, the inner wall grows in non-uniform proportion to the outer wall, making the outer wall difficult to segment.

Segmentation of the outer wall of AAA is particularly challenging due to three main factors. First, in most of the cases, the outer wall is not symmetric around the inner wall. Since only hard structure is in the back of aorta (spine), the aneurysm grows non-uniformly with turbulent flow inside. Some areas have slower flow and develop thrombus lining along the inner wall in that region. This is the reason the outer wall is not always symmetric around the inner wall. Second, the aorta may not always be oval shaped due to the tortuosity and severity of disease, as shown in Fig. 1. Third, there is a lack of color information and a high degree of similarity between foreground (aorta) and background (surrounding tissue).

## Related Work

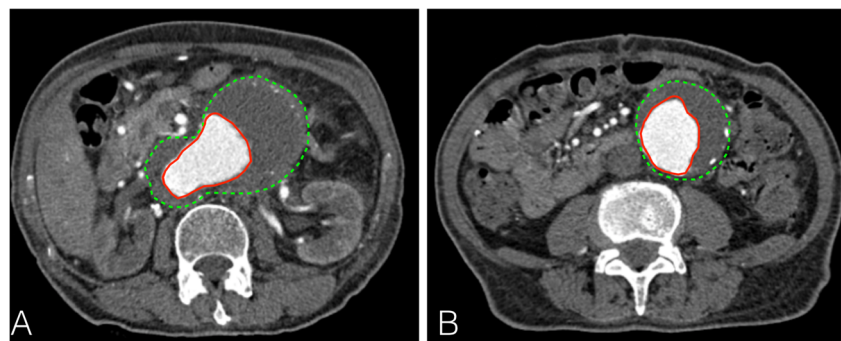
Various imaging modalities have been studied for visualization of aortic aneurysm such as ultrasonography, computed tomography (CT), and magnetic resonance imaging (MRI). Algorithms for aortic wall segmentation can be divided into three categories based on region (thoracic/abdomen), disease (aneurysm/non-aneurysm) and imaging modality. In previous studies, several segmentation algorithms [7–11] were developed for thoracic aorta without aneurysm in non-contrast and contrast enhanced CT. Xie et al. [7] presented an algorithm using anatomical location and cylinder-tracking in non-contrast enhanced CT images of the thoracic aorta. Isgam et al. [8] proposed multi-atlas-based segmentation for non-contrast CT images of thoracic aorta. Kurugol et al. [9, 10] proposed an algorithm to detect the outer wall contour of non-contrast enhanced CT images of thoracic aorta, using anatomical location and circular Hough transform followed by 3D level set segmentation. Raman et al. [11] developed an algorithm to define the outer wall contour of thoracic and abdominal aorta without aneurysm on contrast enhanced CT images by using a minimum cost path through the graph constructed of the pixels. It starts from the inner wall contour and searches a 10-mm search space in the surrounding area. The algorithm was designed for arteries in

patients without aneurysm because the 10-mm search space was not sufficient to find the outer wall contour, whereas a larger search space could have more chance to be confounded by other strong gradient structures such as bone or bowel. The detection of the outer contour for the thoracic region of aorta is not difficult because of the strong gradient difference to the adjacent lung tissue and fat.

A number of studies have addressed segmentations of the aorta with and without aneurysm on MR images [12–16]. Bustamante et al. [12] proposed atlas-based segmentation of thoracic aorta in MR images obtained from different time frames of the cardiac cycle. Herment et al. [13] proposed a 2D deformable surface model in the manually defined region of interest for segmenting thoracic aorta in MR images. Automatic and semi-automatic methods for qualifying wall thickness of the aorta have also been proposed for MR sequences. Adame et al. [14, 15] developed an algorithm to detect inner and outer walls of thoracic aorta without aneurysm and carotid arteries in high resolution MR images. Geographic model-matching is used to find contours using the image gradient information. Wang et al. [16] proposed outer wall segmentation of AAA in MRI using a geodesic active contour (GAC) related method by adding registration-based and prior shape terms to the GAC formulation.

Aneurysm segmentation from CTA is much more difficult than from MR because the CTA is density-based imaging which is not as distinct as the tissue-based MR images. It is well known that the difference between soft tissues is typically clearer on MR than CT images. A number of studies have addressed outer wall segmentation of abdominal aorta on contrast enhanced CT images [17–23]. Shum et al. [17] described a semi-automated algorithm to define wall thickness in patients with AAA based on intensity histograms and neural network segmentation of contrast enhanced abdominal CT images. The outer wall is segmented by the neural network trained on intensity and texture based-features of the images. Shang et al. [18, 19] tracked the outer wall using a semi-automated method by detecting iso-intensity contours in contrast enhanced CT images of abdominal aorta. If isolines do not fully enclose the outer wall boundary, the isolines are eliminated. de Bruijne et al. [20] proposed outer wall segmentation of

**Fig. 1** Examples of CT images of aortic aneurysm in various shapes. **a** Oval shape with eccentric thrombus. **b** Round shape with eccentric thrombus. The dotted green line indicates the outer wall and the solid red line indicates the inner wall



AAA in CTA by manual delineation in the first slice. Then, automatic segmentation of subsequent slices was done using statistical shape model from labeled training images, followed by addition interactive manual delineation. Lee et al. [21] proposed outer wall segmentation of AAA in CTA by graph search based on triangular mesh with additional manual control point. Olabarriaga et al. [22] proposed outer wall segmentation of AAA in CTA using discrete deformable model based on grayscale level information. The grayscale level perpendicular to the boundary was classified into inside, outside and boundary. Zhuge et al. [23] proposed automated level set segmentation of outer wall of AAA in CTA. This level set segmentation required appropriate initial contour as a starting point. Combination of lumen region and possible outer wall region were used to estimate the initial contour. The possible outer wall region was derived from grayscale level. It can be seen that these existing methods [17–22] relied on manual processing. In contrast, this paper investigates the segmentation of the outer wall of AAA using a fully automated process in CTA images.

## Main Contributions

This paper introduces a new method for detection of the outer wall of AAA in CT angiography (CTA), which is currently the most widely used imaging modality in patients with suspected aortic disease, particularly in emergency situations. Grayscale medical images are difficult to be segmented with a single segmentation technique because the pixel similarity between foreground and background objects is very high. In the real situation, many difficult cases were found, which are irregular shaped and abundant soft tissue structures contacting to outer wall. The segmentation of difficult cases is yet an open problem. Thus, this paper focuses on the segmentation of outer wall of AAA in both easy and difficult cases. Our solution is to use two-layer iterative segmentation, alternating between intensity-based and contour-based segmentation techniques. The proposed approach of iteratively combining two different segmentation methods is developed based on the concept of variable neighborhood search (VNS) [24–26]. The basic idea of VNS is to change the neighborhood structure when one algorithm gets trapped in its own local minimum. The second algorithm changes the neighborhood search space to help escape from the local minimum. If the algorithms are properly chosen, a local minimum of one is not a local minimum for the other. In our case, we combine two greedy search algorithms that are both seeking the same solution but are searching in different spaces. By interleaving the two segmentations, they are able to move beyond the local minima and may reach the globally optimal solution. This paper is the first to apply the concept of VNS to solve the problem of grayscale medical image segmentation.

To help with the segmentation of grayscale images, we also introduce a new intensity-based segmentation technique, called graph cut with probability density function (GCPDF). Conventional graph cut or GrabCut [27] is not well suited to grayscale image segmentation because of the lack of information provided by color to distinguish foreground from background. For this reason, graph cut is augmented with a probabilistic model of pixel intensity to assist in discarding undesirable pixel intensities in grayscale images. The contour-based technique applied in this paper is graph cut based active contour (GCBAC) which detects the boundary of an object depending on the gradient difference of the adjacent pixels [28]. In each iteration, GCPDF is used to partition the image using pixel intensity and GCBAC is then used to find the closest boundary in the closed space from the initial contour using pixel gradient. This combination enables segmentation of the outer wall of AAA with high accuracy. The proposed method particularly helps in the case of outer wall contiguous with adjacent soft tissue structures (bowel, psoas muscles) and irregular shape of aneurysm. This study also creates and evaluates the 3D model of AAA using the 2D segmentation results of multiple slices of CT image. The experimental results show an improvement of average accuracy and less variability, when compared with recent studies [18, 19] and existing well-known segmentation techniques [17–22].

## Methods

The image domain  $P$  is partitioned into three regions (as shown in Fig. 2): the aortic lumen  $L$ , the blood clot or thrombosis region  $B$ , and the background  $G$ . Thus,  $P =$

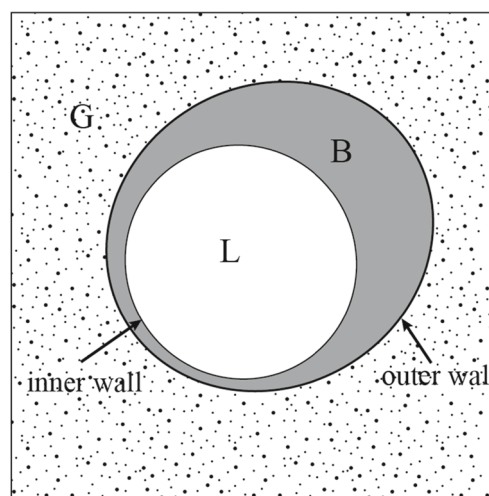


**Fig. 2** Image domain of aortic aneurysm: aortic lumen (**L**), blood clot or thrombus (**b**), background (**g**). The boundary between **L** and **B** is inner wall and the boundary between **B** and **G** is outer wall

$L \cup B \cup G$ . The boundary between **L** and **B** is inner wall and boundary between **B** and **G** is outer wall. The function  $L(p) = Lp : P \rightarrow \{0, 1\}$  is used to define a region in any image  $I$ , where 0 represents the background region and 1 represents the foreground object.

The proposed framework is shown in Fig. 3. The segmentation process begins with segmentation of the **L** region, which can be carried out with simple thresholding because the injection of the contrast medium causes the **L** region to

have a uniform contrast enhancement. Then the inner wall segmentation is carried out as the boundary of the **L** region. The inner wall is then used as a starting point for the next step of segmenting the outer wall. The inner wall is dilated to provide the initial region to be searched for the outer wall. The **B** region between inner wall and outer wall is difficult to segment because it has a pixel intensity similar to the surrounding soft tissue. We utilize the prior knowledge that the intensity in the thrombus (**B** region) is often homogeneous and located adjacent to the aortic inner wall. We leverage this property by first using GCPDF to focus on the segmentation of the area with intensity close to the mean value  $L_{GC}(p) : P \rightarrow \{0, 1\}$ . The GCPDF is used in the first layer of the segmentation because most of the background pixels can be removed at this first segmentation step. This will make the segmentation process faster. The GCBAC is then used to deform the contour to the global optimum (i.e., new contour) in the contour neighborhood  $L_{AC}(p) : P \rightarrow \{0, 1\}$ . The iteration continues with using GCPDF for the first layer segmentation and then GCBAC for the second layer segmentation. The algorithm terminates when the difference between current and previous segmentation results is less than a threshold.

**Preprocessing**

Segmentation of the aortic lumen  $L$  is performed by thresholding  $L_T(p) : P \rightarrow \{0, 1\}$ .

$$L_T(p) = \begin{cases} 1, & \text{if } p \geq \text{thres} \\ 0, & \text{otherwise} \end{cases} \quad (1)$$

where *thres* is the optimum threshold value for the aortic lumen.

To remove small debris after thresholding segmentation, the mathematical morphological operations by Minkowski operation [29] including erosion and dilation are applied. The output is the binary image of the aortic lumen. The erosion of  $A$  by  $B$  is given by the expression [29]

$$A \ominus B = \bigcap_{b \in B} A_{-b} \quad (2)$$

where  $A$  is a binary image and  $B$  is a structuring element in elliptical shape. The dilation of  $A$  by  $B$  is given by the expression [29]

$$A \oplus B = \bigcap_{b \in B} A_b \quad (3)$$

where  $A$  is a binary image and  $B$  is a structuring element in elliptical shape.

The initial contour is mandatory input in the next step. From the binary image of the aortic lumen, this region is dilated to be the initial contour for the next process. Because the outer wall is located beyond the inner wall, the inner wall contour must be dilated to be the initial contour. The size

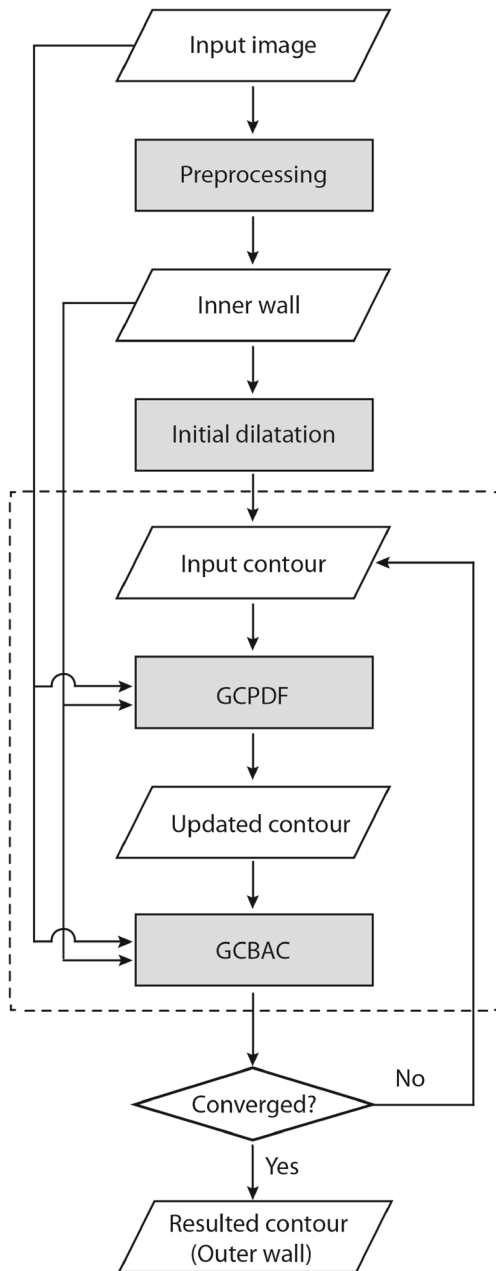


**Fig. 3** Illustration of the proposed framework including two layers of iterative segmentation, composed of graph cut with probability density function (GCPDF) and graph cut based active contour (GCBAC). The input of the segmentation is dilatation of the inner wall of the aorta

of the dilatation is a function of the lumen size, which has been segmented in the preprocessing step. Then the outer boundary of the dilated label  $D$  is the initial contour for the next segmentation.

$$|D| = \alpha|L| \tag{4}$$

where  $\alpha$  is the dilatation factor

### Graph Cut with Probability Density Function

Graph cut is widely used for image segmentation. Its max-flow/min-cut algorithm is applied on the graph to partition the nodes in graph into two groups. The primary data structure for the algorithm is an undirected weighted graph  $G = (V, E)$  composed of a set of nodes  $V$  and a set of directed edges  $E$ . The nodes in  $V$  consist of image pixels  $p \in P$  and two additional terminal nodes: a source  $s$  and sink  $t$  added for processing of graph cut segmentation. The source node  $s$  is used to represent the seed of the foreground, while the sink node  $t$  is used to represent the seed of the background.  $G = (V, E)$  is used for the max-flow/min-cut algorithm in graph cut, as shown in Fig. 4.

A graph cut construction was first used by Greig et al. [30]. Then, Boykov et al. [31] used it to address segmentation in grayscale medical images (e.g., bones and contrast-enhanced kidneys). All pixels in the image are nodes in the graph. Each node has eight n-links and two t-links. For the

segmentation process, seed points (i.e., the brushed region in images) are needed to initially represent the foreground and background regions. Pixel intensities at the seed points are used to create the color model by using a Gaussian mixture model (GMM). One model is used to represent the foreground intensity distributions and another model is used to represent the background intensity distributions. Then, the likelihood to be a source (i.e., the foreground) and likelihood to be a sink (i.e., the background) are computed from these intensity distributions. The n-links are calculated based on pixel intensity similarity. The conventional graph cut algorithm is not well suited to grayscale medical images because the GMMs of the foreground and background are too similar.

To address this problem, we modify the traditional graph cut by adding a probability density function to discard or partition the pixels which have intensity significantly higher or lower than the mean value. The probability density function is used to model the pixel intensity of possible foregrounds. The graph  $G(V, E)$  is constructed with pixels in the region inside the initial contour ( $R_I$ ). The edge weight to the source node  $w(u, s)$  is assigned according to the probability of the pixel intensity of node  $u$  to be a source node using the probability density function. This is shown in Fig. 5.

$$f(x, \mu, \sigma^2) = \frac{1}{\sqrt{2\sigma^2\pi}} e^{-\frac{(x-\mu)^2}{2\sigma^2}} \tag{5}$$

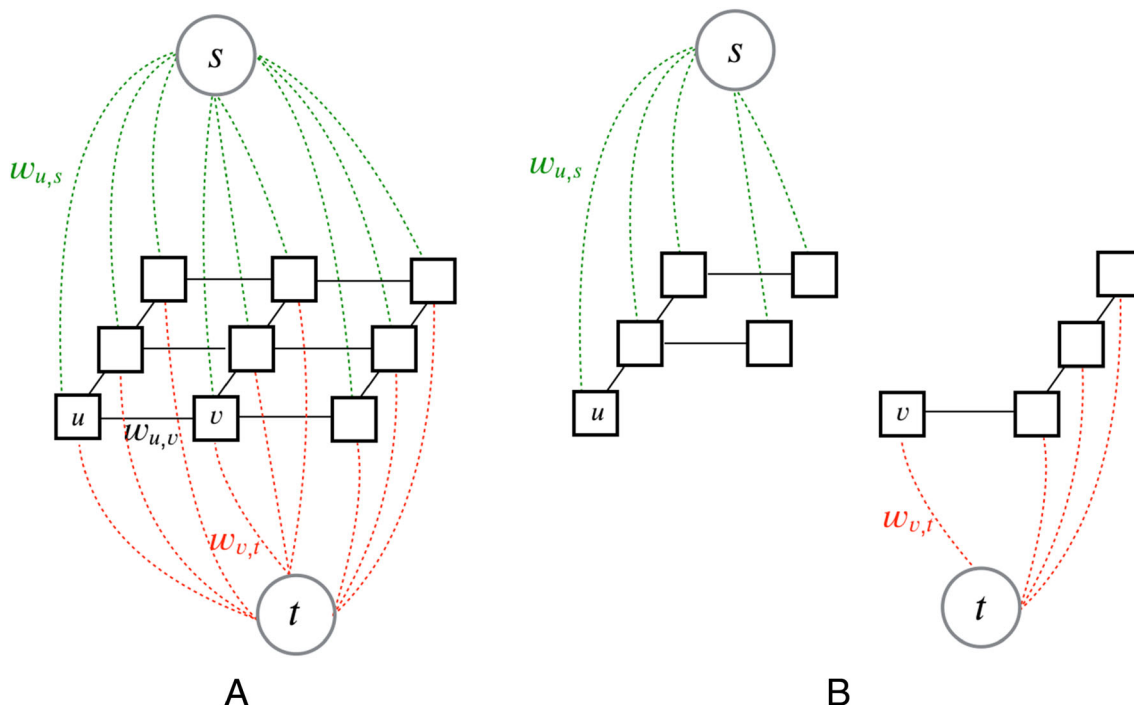
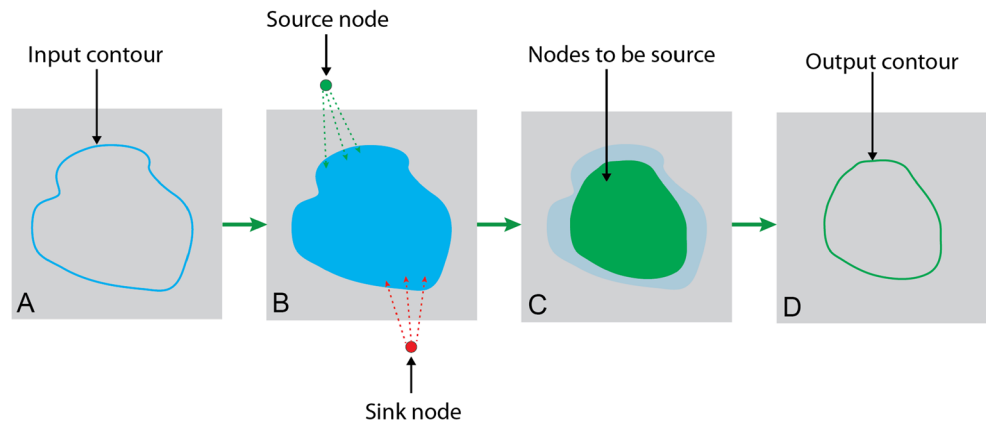


**Fig. 4** Illustration of the graph structure of the graph cut segmentation. **a** All pixels in the image represent nodes ( $u, v$ ) in the graph having weighted edges ( $w_{u,v}$ ) to adjacent nodes, weighted edges to source

( $w_{u,s}$ ) and to sink ( $w_{v,t}$ ). The minimum cut through the edges yields a partition into two regions. **b** Two partitions where one is connected to the source and another is connected to the sink

**Fig. 5** Illustration of graph cut with probability density function. (A) Initial input contour. (B) Graph construction by all pixels inside the input contour. (C) Graph cut segmentation using max-flow/min-cut algorithm. (D) Output contour is outer boundary of partitioning source node



$$\mu = \frac{1}{n} \sum_{i=1}^n (x_i) \tag{6}$$

$$\sigma = \sqrt{\sum_{i=1}^n \frac{1}{n} (x_i - \mu)^2} \tag{7}$$

where  $x$  is the pixel intensity,  $\mu$  is the mean intensity,  $\sigma^2$  is the variance, and  $n$  is the number of pixels in the region inside the initial contour except inner lumen. Then, the pixel intensities are converted to the probability using the probability density function. The edge weight to the source node  $w(u, s)$  is the normalized probability ranging from 0 to 100, and then the corresponding edge weight of the sink node  $w(u, t)$  is  $100 - w(u, s)$ .

The edge weight  $w(u, v)$  is assigned by measuring pixel similarity between two adjacent pixels. The simple image gradient map using standard deviation  $\sigma'$  in small local region ( $3 \times 3$  pixels) is used to measure the pixel similarity, with

$$\sigma' = \sqrt{E[x^2] - (E[x])^2} \tag{8}$$

where  $E[x]$  is the expected value of  $x$ . Then,  $w(u, v)$  is the inverse normalized value of  $\sigma'$  so it ranges from 100 to 0. Simple 4-connectivity to neighborhood pixels is used in the graph. The max-flow/min-cut algorithm is performed

to partition the graph. The output region of segmentation  $R_O = \{p \in P | L_{GC}(p) = 1\}$  defines the region of thrombosis inside the aneurysm. The outer boundary of  $R_O$  is the output contour for the next iteration. From the input contour, the pixels inside the contour are represented by each node in the graph, except the aortic lumen region ( $L$ ). The source and sink nodes are constructed. The weighted edges from node to source, sink and adjacent pixel are calculated. The air and bone regions are also removed pixel by pixel from the graph. The max-flow/min-cut algorithm is performed to partition the graph. The new label is updated to the regions which are connected to the source node to be the outer boundary, as illustrated in Fig. 6.

### Graph Cut Based Active Contour

Graph cut based active contour (GCBAC) is active contour segmentation of an object using graph cut as the optimization tool [28]. In each iteration, the algorithm deforms the initial contour to find the new contour, which is the minimum cut in favor of a shorter boundary. The objective of GCBAC, similar to the classical active contour, is to find the boundary of the object. The classical active contour, also called Snakes [32, 33], has several disadvantages. For instance, Snakes uses a number of

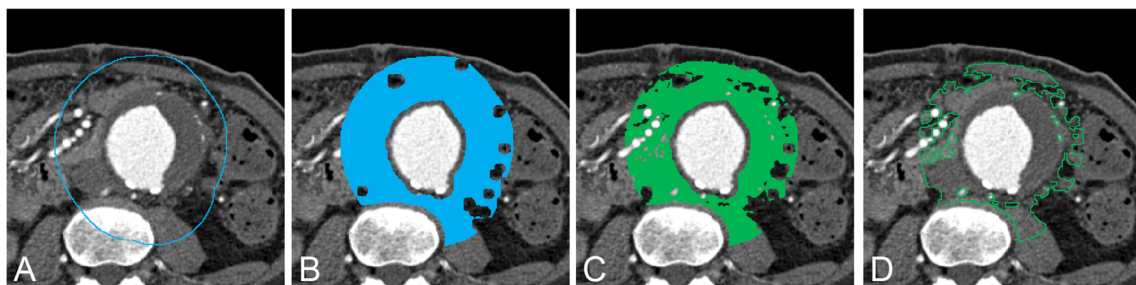
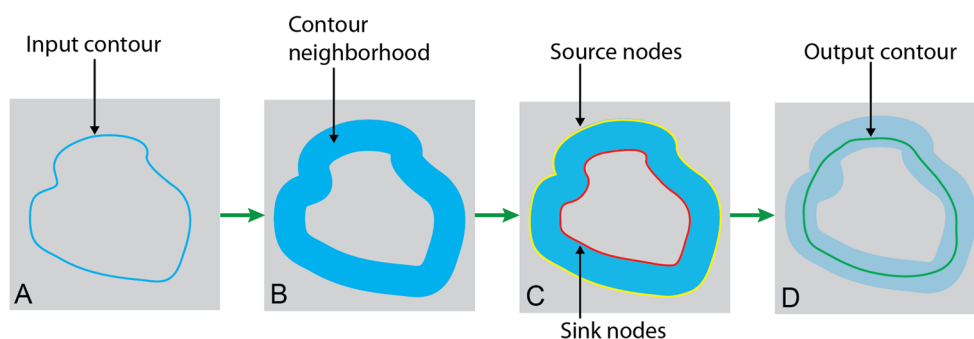


**Fig. 6** An example of graph cut with probability density function corresponding to the diagram in Fig. 5. **a** The initial contour for the segmentation. **b** The label region with bone and air removal. For the graph construction, each pixel in the region is represented by a

node in the graph. **c** The output label region of segmentation using max-flow/min-cut algorithm. **d** The output contour of segmentation corresponds to the outer boundary of **c**

**Fig. 7** Illustration of the graph cut based active contour. (A) Initial with input contour. (B) Dilate input contour to contour neighborhood. (C) Define outer boundary as source nodes and inner boundary as sink nodes. (D) Graph cut segmentation using max-flow/min-cut algorithm to yield the output contour



control points which may lead to unequal spacing or self-crossing during contour deformation. In addition, several parameters to control the Snakes algorithm are difficult to determine. GCBAC is much more practical to find a contour in a desired space or contour neighborhood (CN). Beginning from initial contour, the GCBAC algorithm iteratively dilates the contour to be CN and then finds the new contour within the CN until the contour attains a global minimum. This behavior is similar to Snakes but overcomes some of its limitations. The cost function in GCBAC is minimized by using graph cut. Each pixel in CN represents each node in the graph and edge weight is assigned based on the gradient difference to its adjacent pixels. To solve the problem of global minimum contour within the CN, the pixels on the outer boundary are assigned to be multiple sources and the pixels on the inner boundary of CN are assigned to be multiple sinks. The final contour is the shortest path or max-flow/min-cut in the graph following the concept of the graph cut (Fig. 7).

In the proposed method, the second layer of the segmentation is based on the GCBAC. The output region of segmentation  $R_O = \{p \in P | L_{AC}(p) = 1\}$  defines the region of thrombosis inside the aneurysm. The outer boundary of  $R_O$  is the output contour for the next step of the segmentation. From the input contour, the contour is revised by removing air and bone regions before running GCBAC. The GCABC is performed by dilating the contour into CN. The node in the graph is constructed by using each pixel in

the CN. The max-flow/min-cut algorithm is performed to find the shortest path in the CN and the new output contour is updated, as illustrated in Fig. 8.

## Experimental Results

This experimental study was approved by the institutional review board of Siriraj Hospital, Mahidol University (certificate of approval number: Si 584/2016). The data was obtained from the radiology information system by identifying patients on whom contrast enhanced CTA was performed and who had AAA. In routine practice, CTA is widely used in patients with suspected aortic disease. The exclusion criteria were post open surgery, post endovascular aortic repair, impending rupture, rupture, intramural hematoma, dissection, mycotic aneurysm and poor contrast enhancement of abdominal aortic aneurysm. All CTA acquisition was performed with a 64-slice multi-detector row CT scanner (Somatom Definition; Siemens Medical Systems, Forchheim, Germany or Lightspeed CVT; GE Medical Systems, Milwaukee, Wisconsin, USA). All CTA acquisitions were performed with contrast medium enhancement using non-ionic monomer iodinated contrast medium. The images were reconstructed at 2.5-mm slice thickness. The size of the matrix was  $512 \times 512$  pixels.

The patients were categorized into two groups of ten patients each. The first group contained easy cases for the

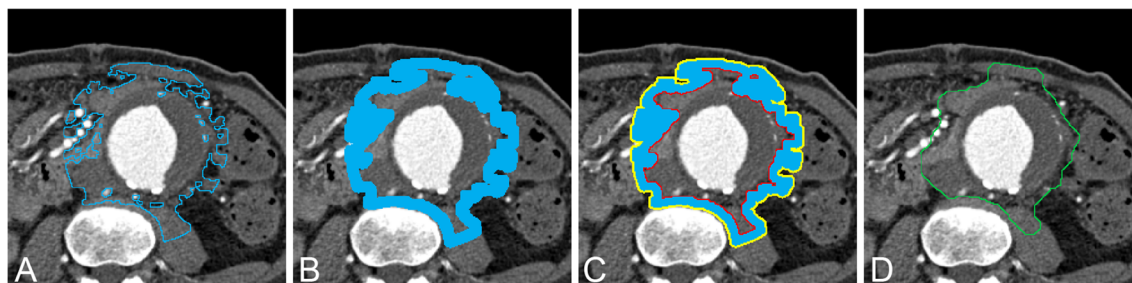


**Fig. 8** An example of graph cut based active contour corresponding to the diagram in Fig. 7. **a** The input contour of the segmentation. **b** Dilate contour to contour neighborhood for the graph cut segmentation. **c**

Label outer and inner boundaries of contour neighborhood to be source and sink nodes, respectively. **d** Output contour of the segmentation

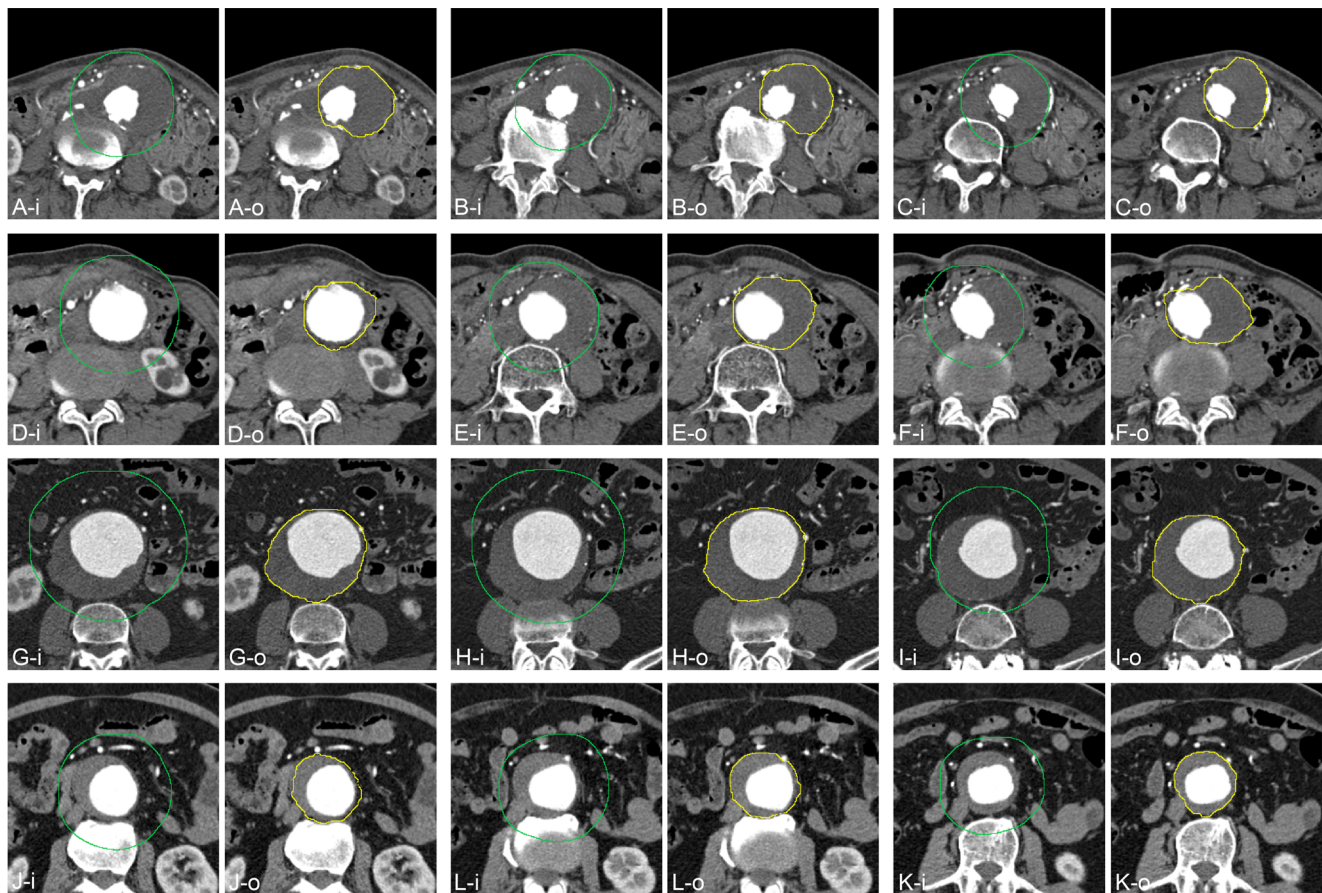


**Fig. 9** Examples of segmentation results at three levels in each of four patients. (A–C), (D–F), (G–I), and (J–K) are groups of images at three levels in the each patient. (X-i) are initial contours for the segmentation. (X-o) are resulted contours of corresponding (X-i) images

segmentation, while the second group contained difficult cases for the segmentation. The easy cases were defined as outer wall non-contiguous with adjacent soft tissue structures (bowel, muscle, other soft tissues), round or minimal oval shaped aneurysm (aneurysm aspect ratio  $\leq 1.2$ ) and thin thrombus (thrombus thickness  $\leq 2.5$  cm). This makes a clear boundary of the outer wall. The difficult cases were defined as outer wall contiguous with adjacent soft tissue structures, pronounced oval shaped aneurysm (aneurysm aspect ratio  $> 1.2$ ) and thick thrombus (thrombus thickness  $> 2.5$  cm). This is difficult partly because the outer wall is in contact with other structures with low gradient and intensity differences at the boundaries. For each patient, five images were selected equally distributed from the beginning to the end of the AAA. We fix the window and level of the CT image for each case at the preprocessing step. The window and level of CT images ranged from 400–700 and 50–150 Hounsfield units, respectively. The source images were converted to 8 bits grayscale. In this experiment, the threshold for the aortic lumen segmentation was manually set and fixed for each

case. The value of the initial dilatation factor  $\alpha$  was set in the range 2 – 4, depending on the size of the aneurysm. This value was set once and used for all slices in each case. The dilatation for CN in GCBAC was fixed to 8 pixels. The algorithm was run on each image until the global optimal contour was found, as shown in Figs. 9, 10, and 11.

Examples of initial contours and segmentation results for easy and difficult cases are shown in Fig. 9. The segmentation terminated after only a few iterations with the resulting contour successfully reaching to the outer wall in easy and difficult cases as shown in Fig. 10. The input, updated, and output contours in each loop of the iterative segmentation progressively converged to the outer wall (Fig. 11). For most of the cases, the contour converged to the outer wall within 10 iterations, which is fast compared with classical active contour alone. The accuracy of the segmentation result was quantitatively evaluated by comparing the segmentation result with ground truth. Ground truth segmentations were obtained by manual segmentation by an experienced cardiovascular radiologist using the GNU image manipulation program (GIMP version 2.8.18).



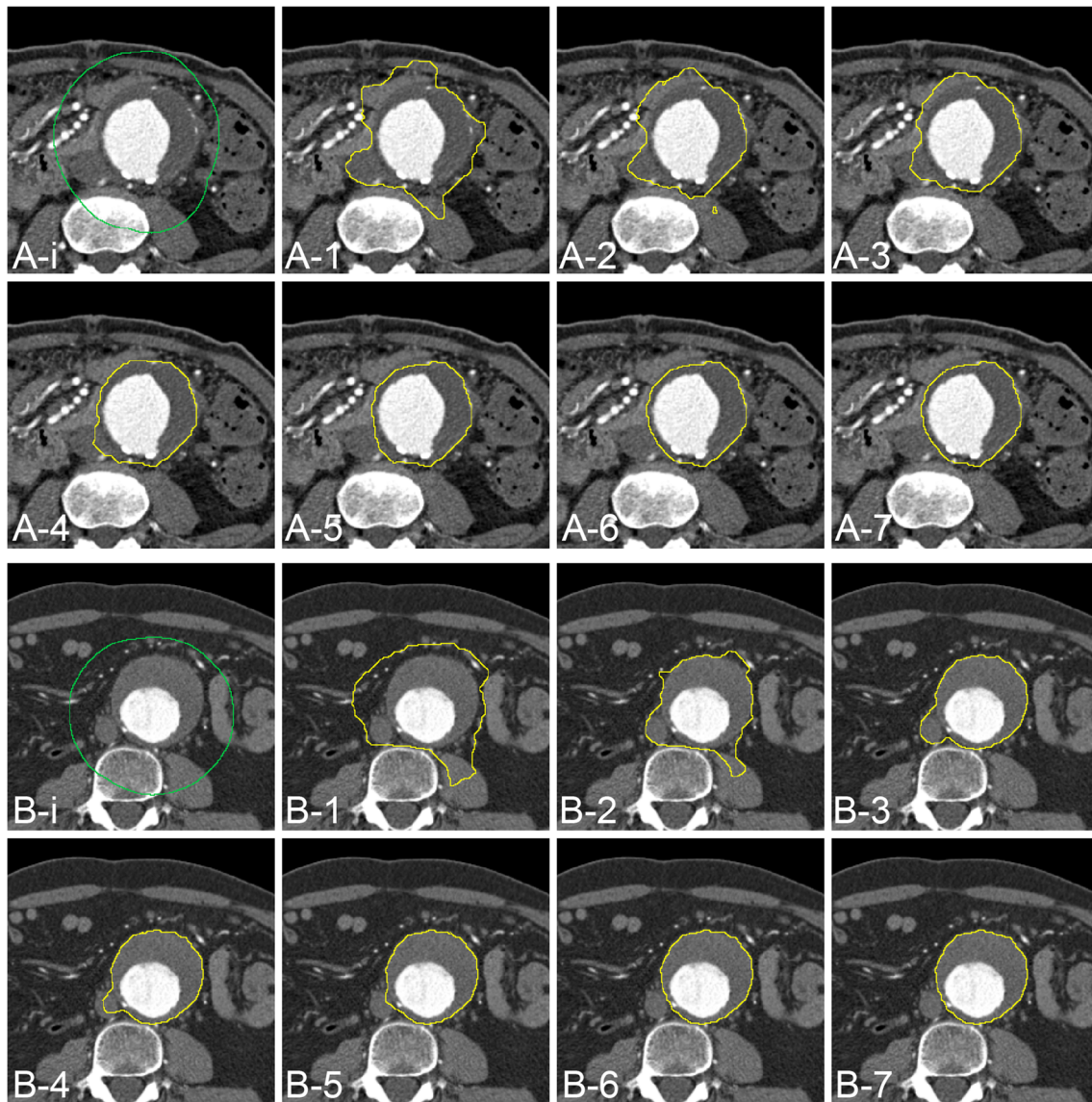


**Fig. 10** Examples of output contours in each iteration. (A-i) and (B-i) are the initial contours for the segmentation in different patients. (A-1) to (A-7) and (B-1) to (B-7) are the output contours of corresponding 1st–7th iterations. (A-7) and (B-7) are the final output contours

The segmentation of contiguous image slices was obtained in two easy and two difficult cases. The sub-selected slices were from the level of renal to iliac arteries using original 1- or 1.25-mm slice thickness (150–200 slices for each case). 3D reconstructions were generated for visualization and data correlation, as shown in Fig. 14. Ground truth segmentations were also obtained by manual segmentation with the 3D slicer version 4.7.0.

The algorithm output was quantitatively compared with ground truth using the dice similarity coefficient (DSC)

$$\%DSC = \frac{2|X \cap Y|}{(|X| + |Y|)} \times 100 \quad (9)$$

and Jaccard similarity coefficient (JSC)

$$\%JSC = \frac{|X \cap Y|}{|X \cup Y|} \times 100 \quad (10)$$

where  $X$  and  $Y$  are regions in an image, which is output from automatic segmentation and ground truth, respectively.

The performance of the proposed method is shown in Tables 1 and 2. For easy cases, the average DSC and JSC are  $94.69 \pm 3.54$  and  $90.11 \pm 5.97\%$ , respectively. For difficult cases, the average DSC and JSC are  $92.71 \pm 5.49$  and  $86.84 \pm 8.60\%$ , respectively. The proposed method was applied to all slices in each case. All methods shown in Tables 1 and 2 were tested on our dataset, so direct

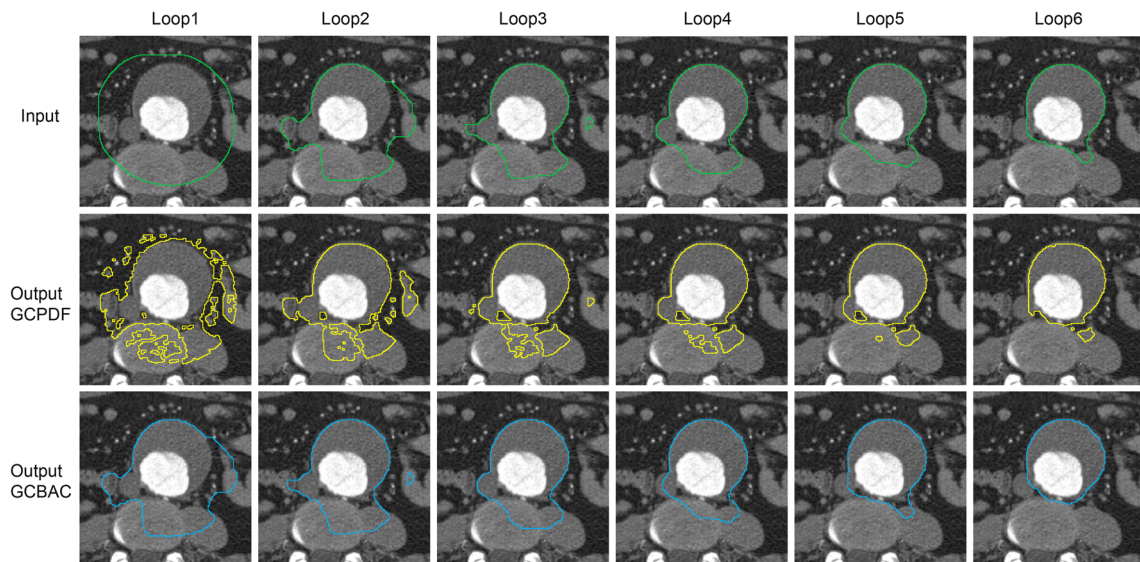


**Fig. 11** Examples of resulting images in each loop of the iterations. The left column is the input contour. The middle column is output contour of the first layer segmentation: graph cut with probability density

function (GCPDF). The right column is output contour of the second layer segmentation: graph cut based active contour (GCBAC). Each row represents each loop of the iteration

comparison can be made. It can be seen that the proposed method significantly outperforms the other existing methods. In addition, for the 3D dataset segmentation of the easy cases, the proposed method achieves average DSC and JSC of 92.47 and 86.00%, respectively. While for the 3D dataset segmentation of the difficult cases, the proposed method achieves average DSC and JSC of 90.11 and 82.03%, respectively. The average number of iterations used for each image in the easy and difficult cases was 8.96 and 10.82, respectively. The minimum number of iterations for any image was 4 and the maximum was 20. The average running time for segmenting each image was only 0.51 and 0.54 seconds (Intel Xeon E5-2697 v3 2.6GHz, 128 GB RAM) for the easy and difficult cases, respectively.

In addition, Table 3 shows performance comparisons on the outer wall segmentation of AAA. The methods shown in Table 3 were tested on different datasets. The performance of the proposed method is shown to be promising when compared with the existing methods. The proposed method is a fully automatic, while the others [17–22] are semi-automatic. Also, the proposed method is shown to work effectively for difficult cases, while the others do not.

### Discussion

The experimental results show high segmentation accuracy of the proposed method (Tables 1 and 2) in both easy (DSC =  $94.69 \pm 3.54\%$ ) and difficult (DSC =  $92.71 \pm 8.60\%$ ) cases. The segmentation results tend to slightly overestimate the outer wall as compared with the manual ground truth because of the strong gradient difference at the rim of the outer wall (Fig. 12). But if the initial contour is underestimated, it will shrink to the inner wall and fail to find the outer wall.

The comparison between the proposed method and other conventional segmentation methods is shown in Fig. 13, Tables 1 and 2. The active contour without edges [34] can detect the nearest object edge from the initial contour but far from the outer wall, with rather low DSC and JSC of  $48.94 \pm 10.46$  and  $33.04 \pm 9.56\%$ , respectively. The distance regularized level set evolution (DRLSE) [35] is more advanced than the classical active contour without edges but can achieve only slightly better results with DSC and JSC of  $59.70 \pm 10.86$  and  $43.44 \pm 11.47\%$ , respectively. Wang et al. [16] reported the accuracy of DRLSE on their

**Table 1** Quantitative evaluation of aortic aneurysm segmentation compared with standard reference (ground truth) using dice similarity coefficient (DSC), based on our dataset. AC = active contour without edges, DRLSE = distance regularized level set evolution, GC = graph cut, GCBAC = graph cut based active contour, GCPDF = graph cut with probability density function

	The proposed method	AC [34]	DRLSE [35]	GC [27]	GCBAC [28]	GCPDF
Easy case	$94.69 \pm 3.54$	$52.24 \pm 9.84$	$59.92 \pm 10.54$	$68.71 \pm 19.35$	$64.86 \pm 16.83$	$66.23 \pm 11.51$
Difficult case	$93.37 \pm 5.45$	$48.94 \pm 10.46$	$59.48 \pm 11.17$	$70.12 \pm 14.63$	$64.26 \pm 16.33$	$63.62 \pm 12.00$
Mean	$93.60 \pm 4.97$	$50.59 \pm 10.24$	$59.70 \pm 10.86$	$69.48 \pm 16.87$	$64.53 \pm 16.49$	$64.81 \pm 11.80$

**Table 2** Quantitative evaluation of aortic aneurysm segmentation compared with standard reference (ground truth) using jaccard similarity coefficient (JSC), based on our dataset. AC = active contour without edges, DRLSE = distance regularized level set evolution, GC = graph cut, GCBAC = graph cut based active contour, GCPDF = graph cut with probability density function

	The proposed method	AC [34]	DRLSE [35]	GC [27]	GCBAC [28]	GCPDF
Easy case	90.11±5.97	35.99±9.70	43.64±11.53	55.62±23.01	50.12±17.75	50.62± 13.28
Difficult case	87.99±6.24	33.04±9.56	43.24±11.41	55.88±17.34	49.44±17.91	47.77±12.96
Mean	88.33±7.67	34.53±9.69	43.44±11.47	55.77±20.02	49.75±17.76	49.06±13.13

datasets with a DSC value of 55.56%, which is similar to its accuracy to our dataset (59.70%).

The classical graph cut can partially detect the outer wall, but other similar intensity pixels in the background are also included. It has DSC and JSC of  $69.48 \pm 16.87$  and  $55.77 \pm 20.02\%$ , respectively. The result of GCBAC alone has DSC and JSC of  $64.53 \pm 16.49$  and  $49.75 \pm 17.76\%$ , respectively. The result of GCPDF alone is similar to the conventional graph cut and GCBAC, with DSC and JSC of  $64.80 \pm 11.80$  and  $49.06 \pm 13.13\%$ , respectively. Among the existing segmentation methods, the conventional graph cut shows the best result. This is because the pixel intensity is useful information for the grayscale segmentation. However, none of the individual segmentation methods is sufficiently accurate in detecting the outer wall for clinical diagnostic purposes.

In fact, the classical active contour or GCBAC works well if the initial contour is close to the object, but this is not possible to achieve in practice. The addition of GCPDF solves this problem since the GCPDF is able to remove unwanted pixel intensity by using its simple probability model. GCPDF brings the contour close enough to the object (Fig. 6) that GCBAC is then able to find the boundary (Fig. 8). Our proposed method was also successfully implemented in contiguous CT slices for 3D model reconstruction. The branching iliac arteries are not a limitation for the proposed segmentation technique (Fig. 14).

Previous studies [16, 20, 22, 23] performed 2D segmentation for each slice of contiguous CT images and then used these to construct a 3D model. The most effective recent method of AAA segmentation [16, 23] is based on active contour such as geodesic active contour or level set. Zhuge et al. [23] proposed level set segmentation of outer wall AAA in CTA. This level set segmentation required an appropriate initial contour as a starting point. Information of known lumen region and possible outer wall region were used to estimate the initial contour. The possible outer wall region was derived from grayscale level. They reported high accuracy of segmentation (95.3%). However, the method required a grayscale level map to generate the initial contour, in which the neighbors connecting to the structure with pixel intensity similar to aneurysmal thrombus were identified as the possible region. If the impossible region has overlap with the aneurysm, it results in missed detection. In our experiment, it is shown that if the initial contour is close to the outer wall, the level set or active contour seems to get the best result. For this reason, it requires a complex algorithm to get the most appropriate initial contour for unknown outer wall.

Wang et al. [16] proposed outer wall segmentation of AAA in MRI using a geodesic active contour (GAC) related method by adding registration-based and prior shape terms to the GAC formation. They reported high accuracy of the segmentation with DSC value ranging from 84.16

**Table 3** Summary of previous and this studies on detection of outer wall of abdominal aortic aneurysm. The methods are tested on different datasets. More details are provided in the discussion section

Detection method	Dataset	Method	Number of test cases	Accuracy (%DSC)	%Error
de Bruijne [20]	CT	Active shape model with intervene manual contour	23	95.8%	3.5–3.9%
Olabarriaga [22]	CT	Discrete deformable model	17	95.0% (82.8–96.8%)	0.4–24.1%
Zhuce [23]	CT	Level set with morphological based initial contour	20	95.3% (92.9–97.5%)	0.04–7%
Lee [21]	CT	Graph search-based with manual control point	9	No DSC reported (success in 4 cases from the total of 9 cases)	–
Wang [16]	MR	Registration based geodesic active contour	19	89.79% (85.35–93.24%)	2.46%
The proposed method	CT	GCPDF+GCBAC	20	93.61% (79.09–98.40%)	4.78%

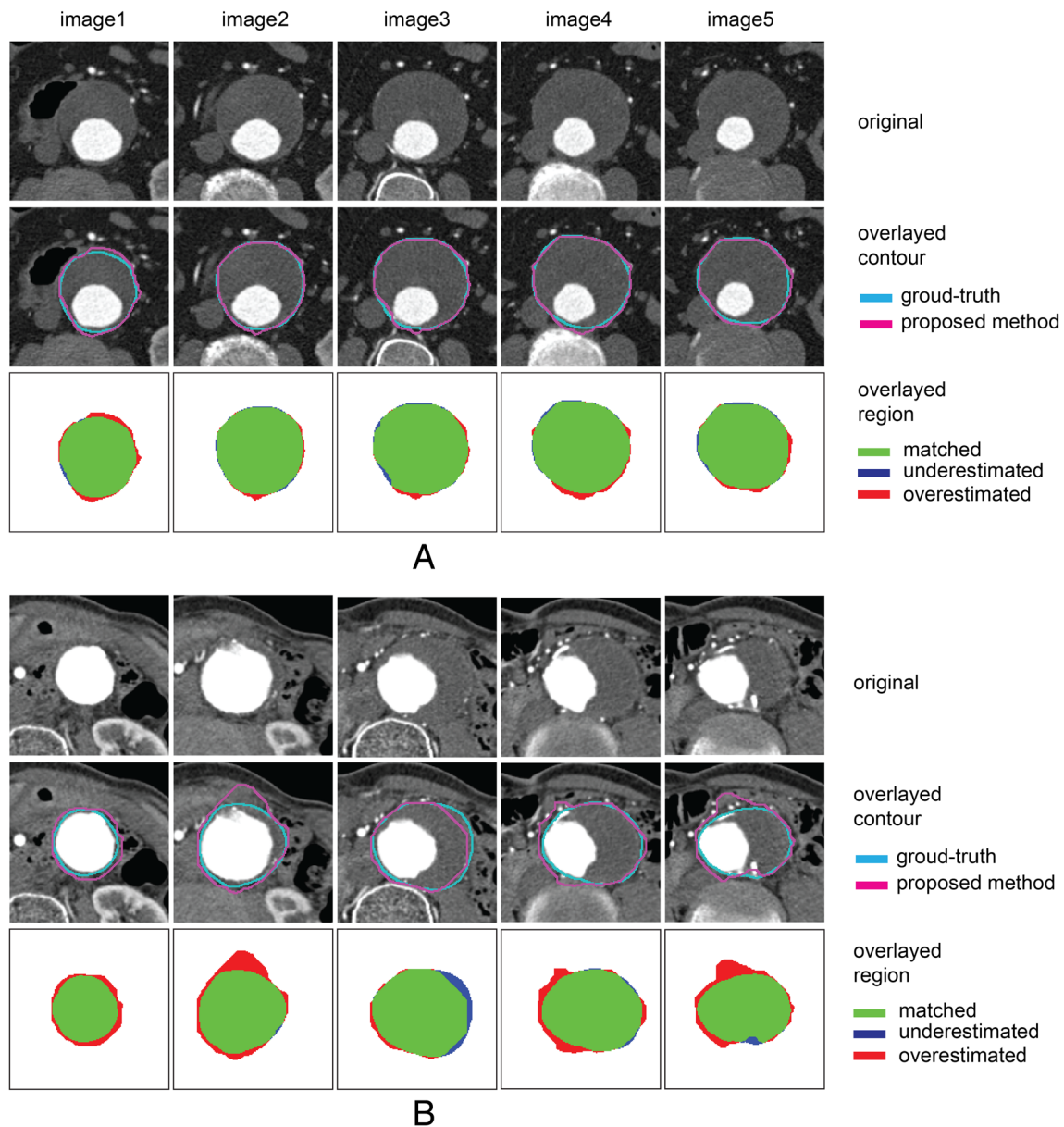


**Fig. 12** Quantitative evaluation of segmentation: The accuracy of the segmentation algorithm is evaluated by comparison with manual segmentation in easy cases (a) and difficult cases (b). The upper row shows original images at five levels of the aorta for each case. The middle row is overlaid contour image, corresponding to the upper row. The cyan color contour represents manual segmentation and the magenta color contour represents the result of the segmentation

algorithm. The lower row shows the areas of overestimation and underestimation of the segmentation algorithm: the green color region shows the area of agreement between the algorithm and manual segmentation, the red color shows the area of overestimation, and the blue color shows the area of underestimation. The dice similarity coefficient for a and b is 96.69 and 90.94%, respectively. The jaccard similar coefficient for a and b is 93.60 and 83.45%, respectively

to 92.27%. Since initialization with manual contour had higher accuracy than automatic Hough circular transform (DSC 90.37 vs 84.16%), they used manual delineation as the initial contour in their experiments. The segmentation result of GAC alone is strongly affected by the initial contour. As previously discussed, results will be good only if the initial contour is close to the foreground object. If the initial contour is far from the object, GAC usually gets trapped by adjacent tissue structure. The level set

or geodesic active contour is contour-based segmentation composed of internal and external energies. The internal energy represents continuity and smoothness of the contour, whereas the external energy is based on image gradient. If the initial contour was inside the aneurysm and the thrombus was large, the final contour usually stopped inside the thrombus. If the initial contour was outside the aneurysm, the final contour was usually stopped at adjacent structures which had stronger gradient difference.

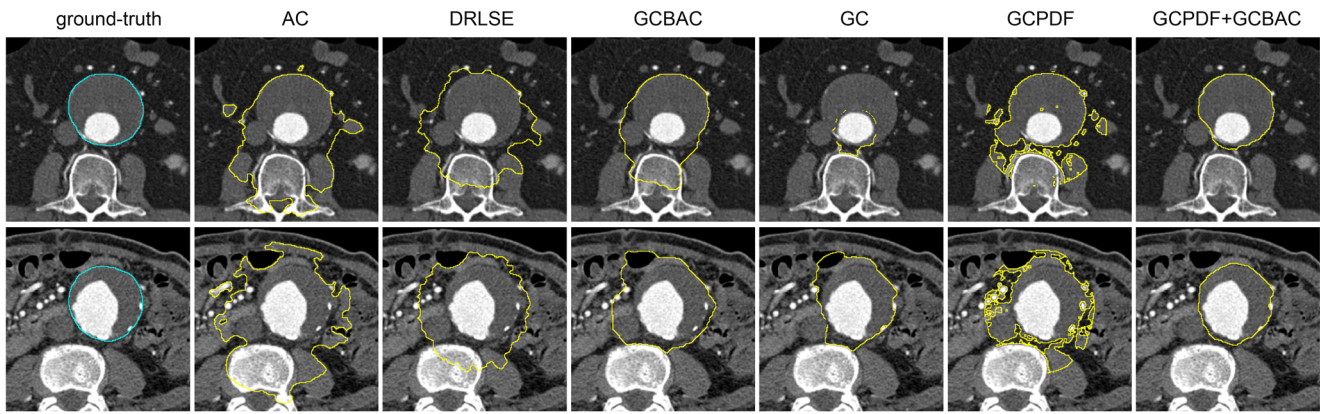


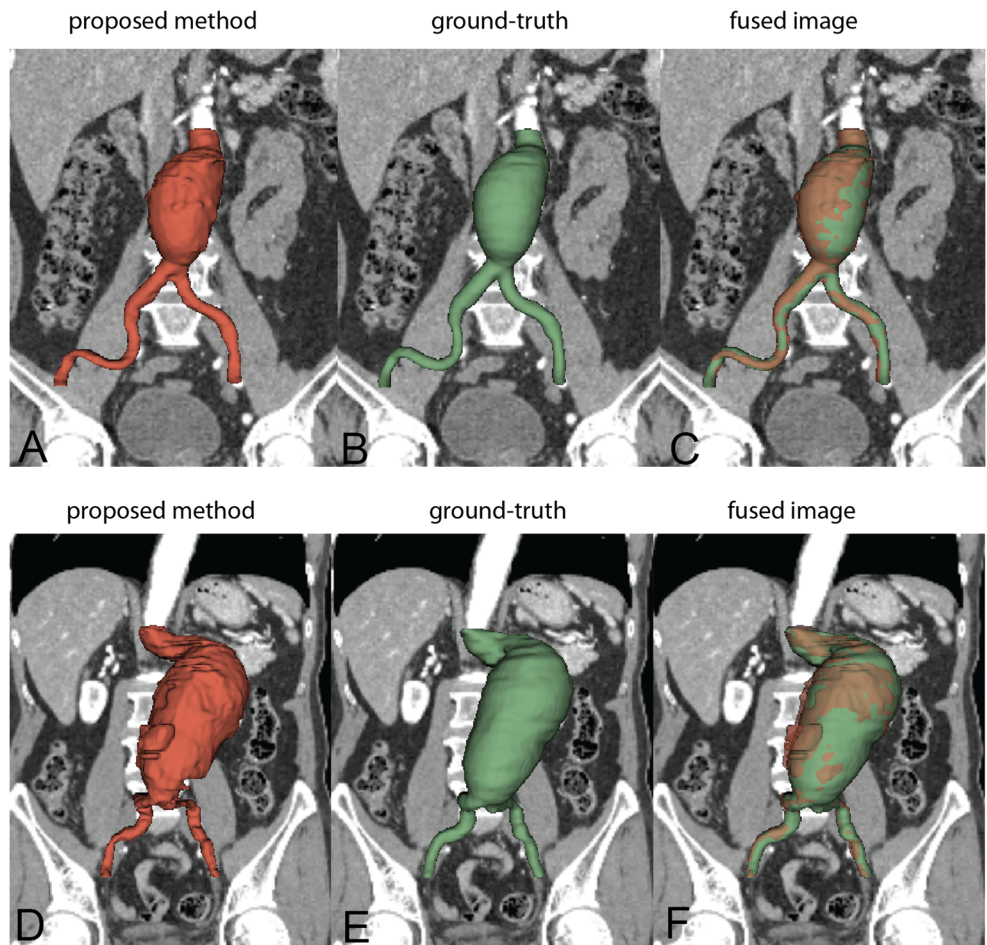
**Fig. 13** Comparison of various segmentations in two different cases. The upper row is a single easy case image and lower row is a single difficult case image. Various segmentation methods are compared with ground-truth (manual segmentation). Conventional active contour (AC), distance regularized level set evolution (DRLSE) and graph-cut based active contour (GCBAC) have similar result but GCBAC is

better. Conventional graph cut (GC) has better result in difficult case and poor result in easy case. Graph cut with probability density function (GCPDF) using single color model has better result in easy case as compared with GC, but the difficult case is worse. Combination of GCPDF and GCBAC has excellent result compared with the other methods and ground-truth

Shang et al. [18, 19] measured the wall thickness of AAA in CT images. They performed simple outer wall segmentation by subsequent growing an isoline from the inner wall. The outer wall was obtained when the isoline

found a large change in intensity reflecting the transition from aorta to surrounding soft tissue. This algorithm has the limitation that if the outer wall is contiguous with adjacent isointensity structures (bowel, muscle, soft tissue)

**Fig. 14** 3D reconstruction of serial 2D segmentations compared with ground-truth. **a–c** An example of easy case with DSC 93.04%. **d–f** An example of difficult case with DSC 91.55%



or aortic wall calcification is present, it usually fails to find the outer wall. They compared aortic wall thickness in 16 aortic surgical specimens with CTA images. The results showed high correlation between image-based and pathologic measurement of wall thickness ( $R = 0.935$ ) in 93.5%. But the error is still high, ranging from  $-12.6$  to  $12.0\%$ .

A number of approaches have made use of partial manual guidance. de Bruijne et al. [20] proposed a method for outer wall segmentation based on active shape model with manually labeled training images. The first slice was segmented by manual delineation. The subsequent slices were segmented automatically using statistical shape model from labeled training images. Then additional interactive manual delineation was used. Olabbarriaga et al. [22] proposed outer wall segmentation by discrete deformable model based on grayscale level model. Manual segmentation was required for training the classifier. They reported high accuracy of the segmentation (95.0%), but the error was still high (0.4–24.1%). The 3D segmentation of outer wall was proposed by Lee et al. [21] by a graph search approach based on triangular mesh. They reported successful segmentation in 4 of 9 cases. Manual intervention was still required in the rest of the cases. Shum et al. [17] measured aortic wall thickness in CT images based on the luminal and outer wall segmentation using commercial software. The reported accuracy of luminal segmentation was 92.5% (with error range of  $-28.19$  to  $65.28\%$ ). They did not report accuracy for the outer wall segmentation. Based on the above discussion, this proposed method achieves the comparable segmentation performance to the previous methods [15, 16, 18]. However, they required manual intervention from the user. In contrast, the method proposed in this paper is fully automatic. This proposed method is also shown to handle difficult cases and cover a longer range of the aorta when compared to these existing methods. However, these previous studies were made on different datasets, which limits the possibility for direct comparison. The time complexity of the proposed method is determined by the complexity of the max-flow/min-cut algorithm used. The complexity for the GCPDF and GCBAC is  $O(n)$  and  $O(n^{1.2})$  [28], respectively, where  $n$  is the number of nodes in the graph. Thus, the total complexity of the proposed method is  $O(n^{1.2})$ .

A limitation of our study is that the neighboring structure with strong edge gradient (spine, bowel) induces the segmentation result to slightly overestimated. For example, in the case of outer wall connecting to the spine, the spine is included in the search space and the segmentation result is stopped at the edge of the spine. Another limitation is at the transition zone between non-aneurysmal and aneurysmal portions of aorta, there is too steep on surface of aneurysm that produces very low edge gradient between outer wall and

adjacent structures. The segmentation result is infrequently underestimated in this region.

## Conclusion

This study has introduced a fully automated process for detection of the outer wall of AAA by using the new concept of VNS that iteratively combines two different segmentation techniques, with one searching through intensity space and the other searching through gradient space. The interleaving combination of GCPDF and GCBAC showed high accuracy for outer wall segmentation in both easy and difficult cases. This novel proposed method for the outer wall segmentation is a highly promising tool to reduce the time and effort to evaluate AAA.

**Acknowledgments** This work was partially supported through a fellowship from the Hanse-Wissenschaftskolleg Institute for Advanced Study, Delmenhorst, Germany to Haddawy for collaborative work with the University of Bremen.

## References

- Sidloff D, Stather P, Dattani N, Bown M, Thompson J, Sayers R, Choke E: Aneurysm global epidemiology study: public health measures can further reduce abdominal aortic aneurysm mortality. *Circulation* 129(7):747–53, 2014
- Sidloff D, Choke E, Stather P, Bown M, Thompson J, Sayers R: Mortality from thoracic aortic diseases and associations with cardiovascular risk factors. *Circulation* 130(25):2287–94, 2014
- Lilienfeld DE, Gunderson PD, Sprafka JM, Vargas C: Epidemiology of aortic aneurysms: i. mortality trends in the united states, 1951 to 1981. *Arteriosclerosis* 7(6):637–43, 1987
- Upchurch GR Jr, Schaub TA: Abdominal aortic aneurysm. *Am Fam Physician* 73(7):1198–204, 2006
- Shum J, Xu A, Chatnuntawech I, Finol EA: A framework for the automatic generation of surface topologies for abdominal aortic aneurysm models. *Ann Biomed Eng* 39(1):249–59, 2011
- Vorp DA: Biomechanics of abdominal aortic aneurysm. *J Biomech* 40(9):1887–902, 2007
- Xie Y, Padgett J, Biancardi AM, Reeves AP: Automated aorta segmentation in low-dose chest CT images. *Int J Comput Assist Radiol Surg* 9(2):211–219, 2014
- Isgum I, Staring M, Rutten A, Prokop M, Viergever MA, van Ginneken B: Multi-atlas-based segmentation with local decision fusion—application to cardiac and aortic segmentation in CT scans. *IEEE Trans Med Imaging* 28(7):1000–10, 2009
- Kurugol S, San Jose Estepar R, Ross J, Washko GR: Aorta segmentation with a 3D level set approach and quantification of aortic calcifications in non-contrast chest CT. In: Proceedings of the Annual International Conference of the IEEE Engineering in Medicine and Biology Society, EMBS, Conference Proceedings, 2012, pp 2343–2346
- Kurugol S, Come CE, Diaz AA, Ross JC, Kinney GL, Black-Shinn JL, Hokanson JE, Budoff MJ, Washko GR, San Jose Estepar R: Automated quantitative 3D analysis of aorta size, morphology, and mural calcification distributions. *Med Phys* 42(9):5467–78, 2015
- Raman B, Raman R, Rubin GD, Napel S: Automated tracing of the adventitial contour of aortoiliac and peripheral arterial walls in CT

- angiography (CTA) to allow calculation of non-calcified plaque burden. *J Digit Imaging* 24(6):1078–86, 2011
12. Bustamante M, Petersson S, Eriksson J, Alehagen U, Dyverfeldt P, Carlhall CJ, Ebbers T: Atlas-based analysis of 4D flow CMR: Automated vessel segmentation and flow quantification. *J Cardiovasc Magn Reson* 17(1):87, 2015
  13. Herment A, Kachenoura N, Lefort M, Bensalah M, Dogui A, Frouin F, Mousseaux E, De Cesare A: Automated segmentation of the aorta from phase contrast mr images: validation against expert tracing in healthy volunteers and in patients with a dilated aorta. *J Magn Reson Imaging* 31(4):881–8, 2010
  14. Adame IM, de Koning PJ, Lelieveldt BP, Wasserman BA, Reiber JH, van der Geest RJ: An integrated automated analysis method for quantifying vessel stenosis and plaque burden from carotid mri images: combined postprocessing of MRA and vessel wall MR. *Stroke* 37(8):2162–4, 2006
  15. Adame IM, van der Geest RJ, Bluemke DA, Lima JA, Reiber JH, Lelieveldt BP: Automatic vessel wall contour detection and quantification of wall thickness in in-vivo MR images of the human aorta. *J Magn Reson Imaging* 24(3):595–602, 2006
  16. Wang Y, Seguro F, Kao E, Zhang Y, Faraji F, Zhu C, Haraldsson H, Hope M, Saloner D, Liu J: Segmentation of lumen and outer wall of abdominal aortic aneurysms from 3d black-blood mri with a registration based geodesic active contour model. *Med Image Anal* 40:1–10, 2017
  17. Shum J, DiMartino ES, Goldhamme A, Goldman DH, Acker LC, Patel G, Ng JH, Martufi G, Finol EA: Semiautomatic vessel wall detection and quantification of wall thickness in computed tomography images of human abdominal aortic aneurysms. *Med Phys* 37(2):638–48, 2010
  18. Shang EK, Nathan DP, Woo EY, Fairman RM, Wang GJ, Gorman RC, Gorman JH, Jackson BM: Local wall thickness in finite element models improves prediction of abdominal aortic aneurysm growth. *J Vasc Surg* 61(1):217–23, 2015
  19. Shang EK, Lai E, Pouch AM, Hinmon R, Gorman RC, Gorman JH, Sehgal CM, Ferrari G, Bavaria JE, Jackson BM: Validation of semiautomated and locally resolved aortic wall thickness measurements from computed tomography. *J Vasc Surg* 61(4):1034–40, 2015
  20. de Bruijne M, van Ginneken B, Viergever MA, Niessen WJ: Interactive segmentation of abdominal aortic aneurysms in cta images. *Med Image Anal* 8(2):127–138, 2004
  21. Lee K, Johnson RK, Yin Y, Wahle A, Olszewski ME, Scholz TD, Sonka M: Three-dimensional thrombus segmentation in abdominal aortic aneurysms using graph search based on a triangular mesh. *Comput Biol Med* 40(3):271–278, 2010
  22. Olabbarriaga SD, Rouet JM, Fradkin M, Breeuwer M, Niessen WJ: Segmentation of thrombus in abdominal aortic aneurysms from cta with nonparametric statistical grey level appearance modeling. *IEEE Trans Med Imaging* 24(4):477–85, 2005
  23. Zhuge F, Rubin GD, Sun S, Napel S: An abdominal aortic aneurysm segmentation method: level set with region and statistical information. *Med Phys* 33(5):1440–53, 2006
  24. Hansen P, Mladenović N: *Developments of Variable Neighborhood Search* Boston: Springer, 2002, pp 415–439
  25. Hansen P, Mladenović N., Moreno Pérez JA: Variable neighbourhood search: methods and applications. *Ann Oper Res* 175(1):367–407, 2010
  26. Mladenović N, Hansen P: Variable neighborhood search. *Comput Oper Res* 24(11):1097–1100, 1997
  27. Rother C, Kolmogorov V, Blake A: Grabcut - interactive foreground extraction using iterated graph cuts. In: *ACM SIGGRAPH 2004 Papers, SIGGRAPH 2004, Conference Proceedings, 2004*, pp 309–314
  28. Xu N, Ahuja N, Bansal R: Object segmentation using graph cuts based active contours. *Comput Vis Image Underst* 107(3):210–224, 2007
  29. Ghosh PK, Haralick RM: Mathematical morphological operations of boundary-represented geometric objects. *J Math Imaging Vision* 6(2):199–222, 1996
  30. Greig DM, Porteous BT, Seheult AH: Exact maximum a-posteriori estimation for binary images. *J R Stat Soc Ser B Methodol* 51:271–279, 1989
  31. Boykov YY, Jolly MP: Interactive graph cuts for optimal boundary & region segmentation of objects in N-D images. In: *Proceedings. Eighth IEEE International Conference on Computer Vision, 2001. ICCV 2001, vol 1, Conference Proceedings, 2001*, pp 105–112
  32. Kass M, Witkin A, Terzopoulos D: Snakes: Active contour models. *Int J Comput Vis* 1(4):321–331, 1988
  33. Maksimovic R, Stankovic S, Milovanovic D: Computed tomography image analyzer: 3D reconstruction and segmentation applying active contour models—'snakes'. *Int J Med Inform* 58-59:29–37, 2000
  34. Chan TF, Vese LA: Active contours without edges. *IEEE Trans Image Process* 10(2):266–277, 2001
  35. Chunming L, Chenyang X, Changfeng G, Martin DF: Distance regularized level set evolution and its application to image segmentation. *IEEE Trans Image Process* 19(12):3243–3254, 2010